

Entropy of the intracluster medium at high redshift

Biman B. Nath

Raman Research Institute, Bangalore 560080, India
(*biman@rri.res.in*)

17 June 2018

ABSTRACT

Recent observations of entropy of intracluster medium (ICM) at high redshift are not consistent with a redshift independent entropy floor. In order to interpret these observations, we study models in which the entropy of ICM is enhanced at the epoch of cluster formation (z_f), which then passively evolves as a result of radiative cooling until the epoch of observation (z_o). We confirm that a z -independent entropy floor is incompatible with the observations. We find that models in which energy deposition into the ICM increases with redshift (scaling approximately as $\sim M_{cl}^{0.6}(1+z_f)^{2.2}$) are consistent with observations of low and high redshift clusters. Possible sources of such non-gravitational heating are briefly discussed.

Key words: Cosmology: Theory—Galaxies: Intergalactic Medium—Galaxies : clusters : general—X-rays: Galaxies: Clusters

1 INTRODUCTION

X-ray observations of ICM in galaxy clusters have shown its entropy to be larger than that expected from pure gravitational processes (Ponman et al. 2003, and references therein). These observations have led to the suggestion that the entropy of ICM has been enhanced. Possible mechanisms for this include ‘preheating’ the gas before its infall into the cluster potential (Kaiser 1991), shock heating during the accretion into the cluster (Tozzi & Norman 2001; Babul et al. 2002; Voit et al. 2003), radiative cooling (Voit & Bryan 2001), and energy input from supernova driven winds (Wu et al. 2000) or active galaxies (Velageas & Silk 1999; Nath & Roychowdhury 2002). Recent observations of lack of an entropy core in the ICM in low mass clusters have been however difficult to interpret in terms of an entropy floor that is expected in ‘preheating’ scenarios (Ponman et al. 2003; Pratt & Arnaud 2003).

Very recently, observations of the ICM entropy at high redshift have shown that a z -independent entropy floor is difficult to reconcile with observations (Ettori et al. 2004). The observed entropy (defined as $S \equiv T/n_e^{2/3}$) is found to scale with redshift as $SE_z^{4/3} \propto (1+z)^{0.3}$ (where $E_z = H(z)/H_0$ is the ratio of Hubble constants at redshifts z and zero). In the Λ CDM universe with $\Omega_0 = 0.3$ and $\Omega_\Lambda = 0.7$, $E_z^{4/3} \propto (1+z)^{0.9}$, which would have led to a stronger scaling of entropy ($SE_z^{4/3}$) with redshift than observed if entropy is determined by a z -independent floor.

It is important to compare these observations with expectations from simple considerations of redshift scaling of various parameters. For example, in the absence of entropy enhancement due to any of the processes mentioned ear-

lier, one expects the clusters forming at high redshift to be denser than their low redshift counterparts, thereby making the entropy lower than at low redshift for a given cluster mass. It is not clear how the requirement of extra entropy should scale with redshift, and this is what we propose to discuss in the present paper.

One important point with regard to the redshift scaling is that these scalings refer to the redshift of observation of a cluster, z_o , whereas any physical model to understand the scaling must involve the formation redshift ($z_f \geq z_o$) of the cluster, as well as the evolution thereafter until z_o (e.g., Kitayama & Suto 1996). In the hierarchical structure formation theory, haloes merge to form bigger haloes as time elapses. Although haloes also become bigger by slow accretion of matter, merging between haloes is the dominant mechanism of driving haloes upward in the hierarchy of structure. In this scenario, there are epochs in between major mergers during which haloes evolve slowly by accretion at a low rate, during which the gravitational potential does not change substantially. In other words, when a cluster is observed at z_o it is reasonable to assume that it has been evolving with a reasonably stable gravitational potential since an earlier epoch, which can be termed its formation redshift $z_f \geq z_o$. Observational scalings of entropy with z_o must therefore be translated to requirements of excess entropy which is likely to depend on the formation redshift z_f , and the duration of evolution between z_f and z_o .

In this Letter, we build models of galaxy clusters formed at high redshift, based on simple extrapolation of those used for clusters formed at the present epoch. We then study the passive evolution of ICM as a result of radiative cooling between the epochs of formation observation. We enhance the

arXiv:astro-ph/0406451v1 21 Jun 2004

entropy of ICM in various ways at its formation redshift and compare with the observations. We then discuss the plausible models of entropy enhancement which are consistent with observations.

Throughout the paper we use the Λ CDM cosmological model with $\Omega_\Lambda = 0.7$, $\Omega_m = 0.3$ and $h = 0.7$.

2 ICM AT HIGH REDSHIFT

We study the distribution of intracluster gas assuming that the total gas mass is very small compared to the total mass of the cluster, and that the gravitational field is dominated by the dark matter. We first determine a ‘default profile’ that the ICM is expected to achieve, in the absence of any non-gravitational modifications to its entropy (§2.1).

2.1 Gas profile without entropy enhancement

We assume the ICM to be initially in hydrostatic equilibrium with the gravitational potential of the dark matter. The dark matter is assumed to follow the universal Navarro-Frenk-White (NFW) profile, $\rho_{dm} = \rho_s / ((r/r_s)(1 + (r/r_s)))$, where $r_s = r_{vir}/c$, ‘ c ’ being the concentration parameter and r_{vir} being the virial radius (Navarro et al. 1997). The virial radius is fixed by the overdensity estimated from spherical collapse model, for the appropriate redshift of the formation of the cluster a_f . The overdensity is approximately given in a Λ CDM universe by $\Delta(z) = 18\pi^2 + 82x - 39x^2$, where $x = \Omega_m(z_f) - 1$ (Bryan & Norman 1998), and whose value at $z = 0$ is approximately ~ 100 ($\Omega_m(z = 0)$ being assumed to be 0.3). The characteristic density ρ_s for a cluster with virial mass M_{cl} is then given by,

$$\rho_s = c^3 \frac{M_{cl}}{4\pi r_{vir}^3} \left[\ln(1+c) - \frac{c}{(1+c)} \right]^{-1}, \quad (1)$$

We use the results of the simulations by Bullock et al. (2001) to estimate the concentration parameter as,

$$c = 9 \left(\frac{M_{cl}}{1.5 \times 10^{13} h^{-1} M_\odot} \right)^{-0.13} (1+z_f)^{-1}. \quad (2)$$

To facilitate the comparison of our results with observations which are often expressed in terms of the radius R_{200} where the overdensity is 200, we compute this radius and present our results in its terms.

We assume, in accordance with the results from numerical simulations by Loken et al. (2002) (see also Borgani et al. (2004); Yepes et al. 2004), that gravitational interaction of baryons with the dark matter gives rise to a ‘universal temperature profile’, which is approximated by $T(r) = 1.33T_{ew} (1 + 1.5r/r_{vir})^{-1.6}$, where T_{ew} is the emission weighted temperature of the cluster. We estimate the emission weighted temperature from the empirical mass-temperature relation for local clusters and include a redshift dependent factor in this relation that is expected from theoretical considerations. The empirical relation found by Finoguenov et al. (2001) is given by,

$$M_{500} = 3.57 \times 10^{13} \left(\frac{k_b T_{ew}}{1 \text{ keV}} \right)^{1.58} M_\odot \quad (3)$$

where M_{500} is the mass contained within the radius where the overdensity is 500. This relation is valid for clusters with

$M_{500} \geq 5 \times 10^{13} M_\odot$ and is a reasonable assumption for the default profile for all clusters.

We have used the temperature profile of Loken et al. (2002) in our calculations because of the convenient analytical fit. It is possible that profiles obtained by other adiabatic simulations (e.g., Borgani et al. (2004)) are somewhat different than the one used here. A temperature profile which is shallower in the inner region than that used here may lead to a slight overestimation of the required excess entropy in the final result (for details of the implications of the ‘universal temperature profile’, see Roychowdhury & Nath 2003).

The expected scaling of the mass-temperature relation with redshift z_f of formation of clusters is $T \propto E_{z_f}^{2/3} M^{2/3}$, where $E_{z_f} = H(z_f)/H(z=0) = [\Omega_0(1+z_f)^3 + \Lambda_0]^{1/2}$ (e.g., Afshordi & Cen 2002). We therefore multiply the observed mass-temperature relation (equation 3) with a factor of E_z^{-1} on the right hand side to determine the default profile at the formation redshift.

The initial gas density profile is then assumed to be determined by the hydrostatic equilibrium condition, $\frac{dp}{dr} = -\rho_g GM(r)/r^2$, where the temperature profile is determined as explained earlier. We normalize the gas density distribution in such a way that the total gas mass within the radius R_{200} is a constant fraction $f_{g,200} = 0.133$ of the total cluster mass, as recently found by Ettori (2003) for high and low redshift clusters.

We express our results in terms of the emission-weighted temperature of the ICM, calculated with the help of the Raymond-Smith code for a metallicity of $Z = 0.3Z_\odot$.

2.2 Enhancement of entropy

We assume two simple methods of entropy enhancement to the initial gas profile. Let us define $\sigma \equiv P/\rho^\gamma$ as the ‘entropy index’, where γ is the adiabatic index. The entropy per unit particle can be written in terms of this entropy index as $s = \text{constant} + (\gamma - 1)k_B \ln(\sigma)$, where k_B is the Boltzmann constant. In terms of this entropy index, we assume that in the first type of entropy enhancement,

$$\sigma(r) = \max(\sigma_0, \sigma_i(r)), \quad (4)$$

where $\sigma_i(r)$ refers to the initial gas profile and σ_0 is a constant, for all radii and for all clusters. Physically, this corresponds to an entropy floor which may be caused by preheating. Below we will refer to this model as the ‘preheating’ case.

In the second type of entropy enhancement, we assume that,

$$\sigma(r) = \eta \sigma_i(r), \quad (5)$$

where η is assumed to be a constant for the given cluster, for simplicity. Physically this type of entropy enhancement would correspond to energy deposition into the ICM after its infall within the cluster potential well. The excess energy per particle thus deposited, $\Delta\epsilon = T\Delta s \propto T \frac{\Delta\sigma}{\sigma} \propto T(\eta - 1)$. Since gas temperature is a weak function of radius, this roughly corresponds to a near uniform deposition of energy throughout the cluster, for a constant value of η . We will refer to this as the ‘post-infall heating’ case in the following.

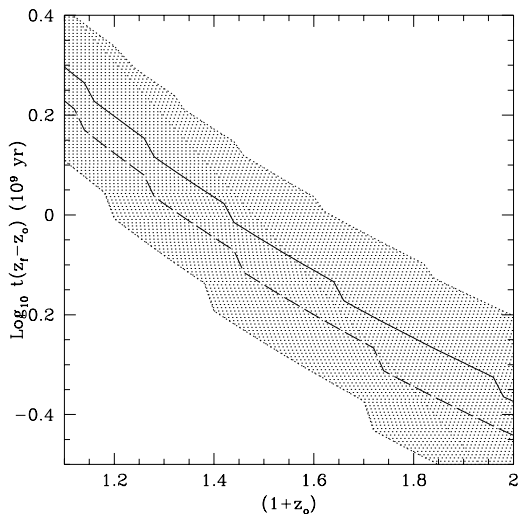


Figure 1. The duration of evolution, between the redshift of formation, z_f and that of observation z_o of clusters of mass $10^{14} M_\odot$ is shown against $1 + z_o$. The thick solid line corresponds to the median value of distribution of z_f and the shaded region corresponds to 30% and 70% values of z_f . The dashed line corresponds to the median value of z_f for clusters of mass $10^{15} M_\odot$.

2.3 Halo formation epoch

Since haloes increase their mass by mergers and steady accretion, it is difficult to assign a single epoch of formation for a given mass. Lacey & Cole (1993) defined the halo formation epoch z_f for a halo of mass M to be the epoch at which the halo has a mass greater than $M/2$ for the first time. After this epoch (‘of formation’) the halo is supposed to attain the total mass M by steady accretion of small objects. Lacey & Cole (1993) then determined the distribution function for the probability that a halo of mass M that is observed at z was formed at z_f , or had a mass greater than $M/2$ for the first time at z_f .

For our calculations, we define the halo formation epoch as the epoch when the halo has a mass greater than $\frac{3}{4}M$ for the first time. This is motivated by the results of numerical simulations which show that gravitational potential does not change much after 75% of the total mass is in place (Navarro et al. 1995; see also Babul et al. 2002).

For our calculations, we use the power spectrum for Λ CDM cosmology normalized by $\sigma_8 = 0.9$, and for growth of linear perturbation in this cosmology, we use the fit by Lahav et al. (1991). Using the probability distribution we can determine different percentiles of the formation epoch z_f . We show in Figure 1 the expected time of evolution, *i.e.* the time spent between the formation redshift z_f and when it is observed at z_o , as a function of z_o for clusters of $10^{14} M_\odot$. The solid line represents the median value of the distribution in z_f and the shaded region the 30% and 70% percentile values. The dashed line shows the median value for z_f distribution for clusters of mass $10^{15} M_\odot$. It is clear that evolution is more important for clusters observed at lower redshifts.

We find that a convenient fit for this duration is given by (for the median value) $\Delta t \approx 2.5 \times 10^9 \text{yr} (1 +$

$z_o)^{-2.6} (M_{cl}/10^{14} M_\odot)^{-0.09}$ which is accurate within 5% for $z_o \leq 1$.

3 EVOLUTION OF GAS IN CLUSTERS

We divide the gaseous sphere (which resides within the potential well provided by the dark matter, $M_{dm} \approx M_T$, which is the total matter) into mass shells which are designated by gas mass contained within them, $M_g(r)$. In terms of the entropy index introduced earlier, the hydrostatic equilibrium condition reads,

$$\begin{aligned} \frac{dP}{dM_g} &= -\frac{GM_T(r)}{4\pi r^4} \\ \frac{dr}{dM_g} &= \frac{1}{4\pi r^2} (P/\sigma)^{-1/\gamma}, \end{aligned} \quad (6)$$

The default profile is computed using these equations and the universal temperature profile. We set the boundary condition that the gas pressure at the mass shell which was at a radius R_{200} for the default profile, and for which $M_g/M_{cl} = f_{g,200} = 0.133$, remains a constant.

The entropy of the gas is then enhanced instantaneously (according to equations 4 and 5). This enhancement changes the density and temperature profile of the gas (pushing it outward to some extent; see below).

We assume that after the initial (impulsive) enhancement, intracluster gas cools radiatively and evolves in a quasi-hydrostatic manner. For subsequent evolution as a result of radiative cooling, if $\Lambda(t)$ denotes the cooling function, the specific entropy evolves with time as (see also Kaiser & Binney 2003),

$$\frac{ds}{dt} = \frac{1}{\gamma - 1} k_B \frac{1}{\sigma} \frac{d\sigma}{dt} = -\frac{\Lambda(T)}{T} n, \quad (7)$$

where the electron density $n_e = 0.85\rho(r)/m_p$. We use the cooling function appropriate for metallicity $Z = 0.3 Z_\odot$ from Sutherland & Dopita (1993) for which Nath (2002) provided a fit. The equation 7 is integrated for each mass shell for a small time interval δt and the entropy index added to this shell after the time interval is,

$$\Delta\sigma = -(\gamma - 1)\sigma n \frac{\Lambda(T)}{k_B T} \delta t. \quad (8)$$

The equations of hydrostatic equilibrium are used again to determine the density and temperature profile at time $t + \delta t$.

4 RESULTS

We first show the results for the case of preheating, *i.e.* the case of an entropy floor (equation 4), in Figure 2. It shows the observed entropy at $0.1R_{200}$ for clusters with different emission weighted temperatures and observed at $z_o = 0.0, 0.5, 1.0$ for an assumed value of $\sigma_0 = 0.27 \times 10^{34} \text{erg cm}^2 \text{g}^{-5/3}$. (For comparison, Tozzi & Norman (2001) used a value of $0.3 \times 10^{34} \text{erg cm}^2 \text{g}^{-5/3}$ for their calculations.) This corresponds to $S \equiv T/n_e^{2/3} \approx 247.9 \text{keV cm}^2$ (assuming $n_e \approx 0.875\rho/m_p$). It is constructed out of data points calculated for clusters of different masses observed at different epochs. The extreme left points in each set correspond to clusters of $5 \times 10^{13} M_\odot$ and the extreme right points use clusters with $5 \times 10^{14} M_\odot$. The thick solid line uses the

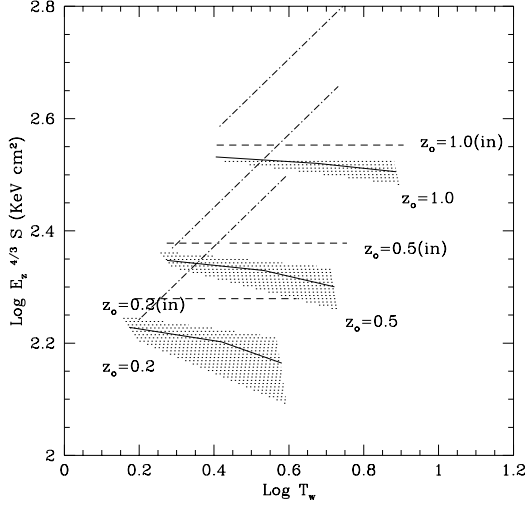


Figure 2. Plot of entropy (at $0.1R_{200}$) for clusters with different T_{ew} and observed at redshifts $z_o = 0., 0.5, 1.0$. The thick solid lines in each redshift set correspond to the median value of distribution of z_f and the shaded region (with dots) to the range between 30% and 70% values of z_f . For comparison, the initial entropy of the same clusters are shown with dashed lines (and labeled ‘in’). The three slanted dotted lines show the observed scaling of entropy-temperature relation, $E_z^{4/3} S \propto T^{0.65}(1+z_o)^{0.3}$, corresponding to the three different redshifts $z_o = 0., 0.5, 1.0$.

median value of distribution of z_f , and the shaded region corresponds to the range between 30% and 70% values of z_f .

Figure 2 leads to a few important conclusions. Firstly, it is clear that a z -independent entropy floor is inconsistent with both the observed S-T relation at low redshift and its scaling with redshift. The S-T relation that follows from it is in general shallower than the observed $S \propto T^{0.65}$ scaling at the present epoch (Ponman et al. 2003). This result has been earlier noted by Borgani et al. (2001) from numerical simulations. The evolution of ICM between the formation redshift and that of observation makes this problem worse. This is because gas in massive clusters (with higher T_{ew}) loses entropy at a faster rate. This is elaborated in Figure 3, which shows a few examples of evolutionary tracks of entropy with redshift for different clusters with various z_f . The solid and the dotted lines show the evolution of a massive and poor cluster, respectively, with the same z_f . Clearly the ICM in massive cluster loses entropy faster than the ICM in low mass clusters, making the observed S-T relation in Figure 2 flatter than the initial S-T relation at formation. Moreover, since the duration of evolution (between z_f and z_o) is longer at low redshifts, the flattening of S-T relation is prominent at lower redshifts.

Secondly, the evolution of the S-T relation with redshift is stronger than observed (shown with dotted lines). This has already been pointed out by Ettori et al. (2004). Our calculations show that the problem is made worse than previously thought as a result of evolution of ICM between z_f and z_o .

We then turn to the case of post-infall heating. We have found that assuming η to be independent of cluster mass and redshift produces a steeper S-T relation than observed, and

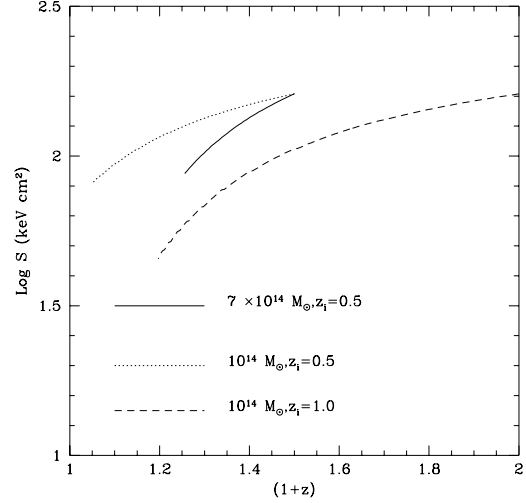


Figure 3. Evolution of entropy at $0.1R_{200}$ for clusters of different masses with different redshifts of formation is shown. Dotted and dashed lines correspond to clusters of mass $10^{14} M_\odot$ with formation redshift 0.5 and 1.0 respectively, and solid line correspond to, $5 \times 10^{14} M_\odot$ with $z_f = 0.5$.

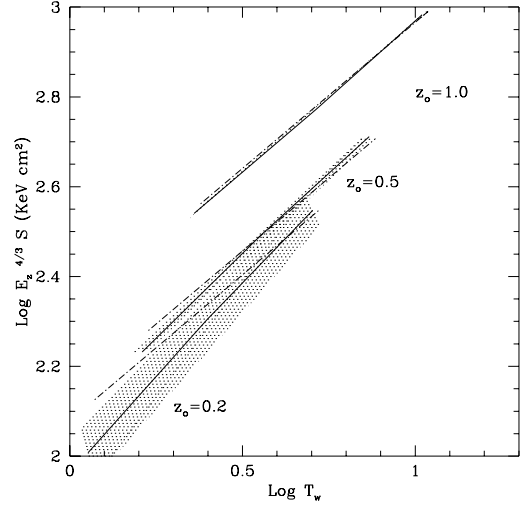


Figure 4. Same as in Figure 2 but for the case of ‘post-infall’ entropy enhancement, with $\eta \propto M_{cl}^{-0.3}(1+z_f)^{2.2}$.

a scaling with redshift slower than observed. We therefore used simple power-law scalings for η with cluster mass and redshift in the form, $\eta(M_{cl}, z_f) \propto M_{cl}^\alpha(1+z_f)^\beta$, and determined the approximate values of α and β that produce results consistent with observations.

We show in Figure 4 the results for the ‘post-infall’ heating case, with $\eta = 10 (M_{cl}/5 \times 10^{13} M_\odot)^{-0.3}(1+z_f)^{2.2}$, along with the observed S-T relation and its scaling with redshift (shown with dotted lines). We find that this form of dependence of η with cluster mass and formation redshift is reasonably consistent with observations.

Finally, we show a few examples of the entropy profiles, before and after the entropy enhancement and after the passive evolution until the epoch of observations, for a couple of clusters with varying masses in Figure 5. The

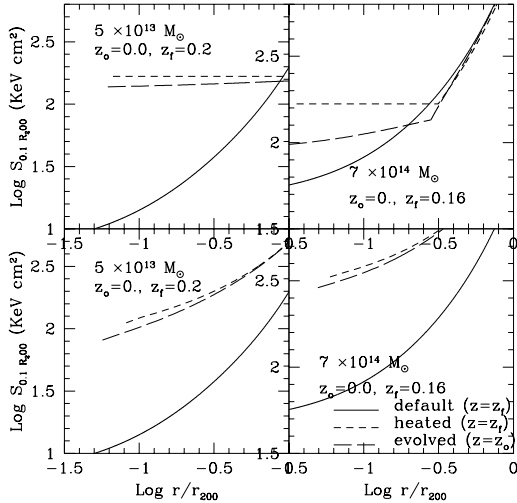


Figure 5. Entropy ($S = T/n_e^{2/3}$) profiles are shown at different epochs for two types of entropy injection and for two cluster masses. The left panels represent clusters of mass $5 \times 10^{13} M_{\odot}$ with $z_f = 0.2$ and the right panels, $7 \times 10^{14} M_{\odot}$ $z_f = 0.16$. The upper panels show the case of z -independent entropy floor (equation 4) and the lower panels show the case of ‘post-infall’ heating (equation 5). The solid curves show the initial profile, the dashed lines show the profile immediately after entropy injection and the long-dashed curves show the result of evolution until the redshift of observation at $z_0 = 0$.

solid line shows the initial entropy ($S \equiv T/n_e^{2/3}$) profile at formation epoch. The dashed curve then shows the profile after entropy enhancement. The upper panels show the result of using equation (4) for entropy injection and the lower panels use equation (5). As expected, the intracluster gas is pushed out as a result of this entropy injection. Finally the long dashed curves show the result of evolution until the redshift of observation ($z_0 = 0$ in this case). The left panels show the case of $M = 5 \times 10^{13} M_{\odot}$ and the right panels that of $M = 7 \times 10^{14} M_{\odot}$. The redshift of formation for these two cases have been chosen to be the corresponding median values of distribution of z_f (0.16 and 0.20).

5 DISCUSSION

We discuss the implication of the result arrived at the last section that energy deposition in ICM with $\eta \propto M_{cl}^{-0.3}(1+z_f)^{2.2}$ is consistent with observations of low and high- z clusters. Firstly, since the excess energy deposited per particle is proportional to $T(\eta - 1) \sim T\eta$ (since $\eta > 1$), our assumption of a constant η for a given cluster roughly amounts to uniform deposition of energy throughout the cluster, since temperature is a weak function of radius (it decreases by much less than an order of magnitude from the core to the outermost radius for the default profile). Secondly, since $T \propto M_{cl}^{2/3}$, the variation of η with M_{cl} implies that the required energy per particle $T\eta \sim 10 \text{ keV } M_{cl}^{1/3}$. Since gas mass is proportional to the total mass, the above result implies that the total required amount of energy $\Delta E \propto \Delta \epsilon M_{cl} \propto M_{cl}^{1.3}$.

The required scaling of η with redshift ($\propto (1+z_f)^{2.2}$) is mainly due to the fact that densities are larger at higher redshift, reducing the default entropy level, and thereby in-

creasing the requirement. This increase is somewhat compensated by the relatively short duration of evolution (between z_f and z_0) at high redshift (see Figure 1) but not significantly.

It is of course possible that the enhancement of entropy is more complicated than represented by equations 4 and 5. Especially the form of energy deposition into the ICM after its infall can either depend on the radius and/or time, in which case the required scaling of η would be different from the results presented here. A non-trivial radial dependence of η may change the entropy profile substantially and change the form of passive evolution thereafter. For example, in the case of a strong radial dependence, the entropy in the inner region may increase substantially, with the possibility of a negative entropy gradient ushering convective flows (e.g., Roychowdhury et al. 2004).

Our assumption of an instantaneous entropy enhancement followed by passive evolution has been admittedly simple, since our goal has been to interpret the general dependence of observed entropy with redshift. It is however possible that the period of entropy enhancement is substantial (see, e.g., Roychowdhury et al. 2004), but modelling such cases introduces another free parameter (of enhancement timescale) in the calculation. Although detailed modeling of such complicated forms of heating may change the scaling power index of η with redshift to some extent, but is not expected to substantially change the strong redshift dependence of η , which mainly arises from densities being larger at high redshift.

It is interesting to note that the final entropy profiles in the case of near-uniform heating after infall (see lower panels of Figure 5) are consistent with recent observations of positive gradient of entropy even at small radii for poor clusters, instead of a core as expected from the preheating scenarios (upper panels of Figure 5) (Ponman et al. 2003; Pratt & Arnaud 2003). The near isentropic core in the case of an entropy floor is consistent with the numerical simulations of Borgani et al. (2001) (considering that the value of the entropy floor used here is larger than assumed by them), and also Babul et al. 2002 (who used a value of σ_0 that is 1.7 times that used here). We must however remember that a strong radial dependence of heating of ICM may change the profile by depositing more energy (and entropy) in the central region as compared to the outer region. In other words, the recent observations of positive gradient of entropy at inner radii is consistent with a (post-infall) near-uniform energy deposition into the ICM throughout the cluster.

As far as the plausible sources of heating which can explain the observations of high redshift ICM, it is interesting to note that rate of heating by active galaxies is expected to rise with redshift (Nath & Roychowdhury 2002) mainly because of the fact that quasar activity has declined in the universe in the recent past. The amount of energy deposited is also reasonably consistent with estimates from heating from buoyant bubbles from active galaxies (Roychowdhury et al. 2004). In this regard, one should also consider the possibility of supernova driven winds as the source of heating, since the total energy deposited in this case is also expected to increase with the cluster mass (total mass of galaxies, from which the winds would emanate, being proportional to the total cluster mass). Moreover since the average star formation rate in the universe increases with redshift (for

$z \leq 1$), it is possible to achieve a strong redshift dependence in this case. We however note that detailed calculations have shown supernova driven winds to be inefficient sources of heating (Wu et al. 2000).

6 SUMMARY

We have calculated the expected evolution of entropy of ICM (at $0.1R_{200}$) with redshift (of observation z_o), taking into account passive evolution of ICM between the epochs of formation and observation of the cluster. We found that the adoption of a z -independent entropy floor exacerbates the problem of accounting for the observed evolution of the entropy-temperature relation with redshift. If the entropy is enhanced instead with the help of a heating source after the infall of the ICM, we find that the total energy required to be deposited scales as $\Delta E \propto M_{cl}^{1.3}(1+z_f)^{2.2}$.

It is a pleasure to thank S. Roychowdhury and S. Sridhar for stimulating discussions, and the anonymous referee for valuable suggestions.

REFERENCES

- Afshordi, N., & Cen, R. 2002, ApJ, 564, 66
 Babul, A., Balogh, M.L., Lewis, G.F., & Poole, G.B. 2002, MNRAS, 330, 329
 Borgani, S., Governato, F., Wadsley, J., Menci, N., Tozzi, P., Lake, G., Quinn, T. & Stadel, J. 2001, ApJ, 559, L71
 Borgani, S. et al. 2004, MNRAS, 348, 1078
 Bryan, G. L., & Norman, M. L. 1998, ApJ, 495, 80
 Bullock, J.S. et al. 2001, MNRAS, 321, 559
 Ettori, S. 2003, MNRAS, 344, 13
 Ettori, S., Tozzi, P., Borgani, S. & Rosati, P. 2004, A&A, 417, 13
 Finoguenov, A., Reiprich, T. H., & Böhringer, H. 2001, A&A, 368, 749
 Kaiser, N. 1991, ApJ, 383, 104
 Kaiser, C. R., & Binney, J. 2003, MNRAS, 338, 837
 Kitayama, T. & Suto, Y. 1996, ApJ, 469, 480
 Lacey, C., Cole, S. 1993, MNRAS, 262, 627
 Lahav, O., Rees, M. J., Lilje, P. B., Primack, J. R., 1991, MNRAS, 251, 128
 Loken, C., Norman, M.L., Nelson, E., Bryan, G.L., & Motl, P. 2002, ApJ, 579, 571
 Nath, B.B. 2003 MNRAS, 339, 729
 Nath, B. B. & Roychowdhury, S. 2002, MNRAS, 333, 145
 Navarro, J. F., Frenk, C. S., & White, S. D. M. 1997, ApJ, 490, 493
 Ponman, T.J., Sanderson, A.J.R., & Finoguenov, A. 2003, MNRAS, 343, 331
 Pratt, G. W. & Arnaud, M. 2003, A&A, 408, 1
 Roychowdhury, S., & Nath, B.B. 2003, MNRAS, 346, 199
 Roychowdhury, S., Ruzsowski, M., Nath, B. B. & Begelman, M. C. 2004, preprint (astro-ph/0401161)
 Sutherland, R.S., & Dopita, M.A. 1993, ApJS, 88, 253
 Tozzi, P., & Norman, C. 2001, ApJ, 546, 63
 Valageas, P., & Silk, J. 1999, A&A, 350, 725
 Voit, G.M., & Bryan, G.L. 2001, Nature, 414, 425
 Voit, G. M., Balogh, M. L., Bower, R. G., Lacey, C. G. & Bryan, G. L. 2003, ApJ, 593, 272
 Wu, K.K.S., Nulsen, P.E.J., & Fabian, A.C. 2000, MNRAS, 318, 889
 Yepes, G., Ascasibar, Y., Sevilla, R., Gottlöber, S., & Müller, V. 2004, in Proceedings of IAU Coll. no. 195 (A. Diaferio, Ed.), in press (astro-ph/0404556)